8. National Conference on Computational Mechanics
MekIT'15
B. Skallerud and H I Andersson (Eds)

A STUDY ON THE COUPLING BETWEEN ISOTROPIC TURBULENCE AND HETEROGENEOUS REACTIONS

Jonas Krüger[1], **Nils E. L. Haugen**[2], **Terese Løvås**[1] **and Dhrubaditya Mitra**[3]

[1] *NTNU EPT, Trondheim, Norway*
[2] *SINTEF Energy Research, NO-7465 Trondheim, Norway*
[3] *Nordita, KTH Royal Institute of Technology and Stockholm University, Roslagstullsbacken 23, SE-10691 Stockholm, Sweden*

Key words: DNS, Particle Clustering, Passive Scalar, Heterogeneous Reaction

Abstract. The effect of turbulence and particle clustering on the decay rate of a chemically reacting scalar is studied with direct numerical simulations (DNS). The scalar is consumed on the surface of the particles. When the chemical timescale is of the same order or less than the particle time scale, particle clustering slows down the scalar decay rate. This effect is present for all turbulence intensities and particle Stokes numbers, as long as the Damköhler number is sufficiently large. For the present studies, turbulent diffusivity plays a minor role in comparison to the molecular diffusivity.

1 Introduction

Coal based fossil energy production will continue to play a major role in the foreseeable future [1]. Therefore, strong efforts to improve its efficiency and decrease its environmental impact through computer aided design are required. This calls for a solid understanding of the multitude of processes involved. The main processes during fossil fuel energy production are flow turbulence, radiation and homogeneous and heterogeneous reactions. The industry already uses a wide span of models for flow turbulence of different levels of detail, and more sophisticated and costly models become usable as the available computers become cheaper and faster.
Reynolds-averaged Navier Stokes (RANS) studies using different submodels for the Reynolds stress term such as $k-\epsilon$ or Reynolds stress modeling (RSM) are used together with global homogeneous and heterogeneous mechanisms to simulate the performance of an actual gasifer [2]. Since the RANS approach does not compute the instantaneous velocities, the particles were dispersed using a stochastic tracking scheme. This scheme only influences the trajectory of the particle, having no direct effect on the reaction rate.
The group of Abani uses Large Eddy Simulation (LES) with a three-step heterogeneous mechanism to simulate coal gasification [3]. They account for the interaction between fluid and solid via a moving flame front model, where the overall heterogeneous reaction rate is a combination of a kinetic rate given

Corresponding author: jonas.kruger@ntnu.no

by an Arrhenius expression and a diffusion rate dependent on the temperature between the particle and the surrounding fluid. Results include temperatures, species mass fractions and particle distribution in a coal-oxygen jet and compare them with lab-scale gasifier measurements. It has to be noted that the usage and sophistication of LES tools is expected to increase [4] [5]. Even a Direct Numerical Simulation (DNS) of pulverized coal flames with a three-step char reaction mechanism, Reynolds numbers up to 28,000 and accounting for devolatilization is reported by the group of Luo et al. [6]. They obtained for example heat release rates and particle distributions at different planes along a pulverized jet flame and compared against experiments.

Chemical mechanisms and models for homogeneous combustion in turbulent flows are widespread and cover the range of combustion regimes, from laminar to turbulent and from non-premixed to premixed flames [7], [8]. It is apparent that the field of heterogeneous combustion modeling has not seen as extensive development as its homogeneous counterpart.

overall 1,2:give overview about previous studies and emphasize what is new, objectives of the study specific p1: give reference to a RANS methodology of the studies

In all of the studies mentioned, the effect of turbulence on the particles trajectory is accounted for, either by a model [2] or directly by the instantaneous velocity of the fluid [6]. The coupling of flow turbulence, resulting clustering and heterogeneous reaction rates at the surface of particles are not looked at due to the inability of the employed model to capture clustering (except in the work of Luo [6]). This study aims at providing some insight into how particle cluster depending on flow attributes in a flow with no preferential direction, and how this influences the fluid-solid interaction. Especially the resulting overall reaction rates when particles cluster together and rapidly consume fluid reactants inside volumes where a lot of particle are present are looked at and upper boundaries for these reaction rates are reported. This is done to work towards a heterogeneous combustion model for RANS or LES Computational Fluid Dynamics (CFD) that accounts for two-phase flows with varying particle number densities, particle compositions and turbulence intensities in one domain.

The system analysed is very simple to reduce computational cost and to avoid secondary effects from other flow attributes such as temperature, changing diffusivities and reaction paths. The complexity of the flow can be increased when the basic laws governing the heterogeneous reactions are better understood.

2 Theory

We look at a simple isothermal flow field with isotropic turbulence that is governed by the continuity equation

$$\frac{\mathrm{D}\rho}{\mathrm{D}t} = -\rho \boldsymbol{\nabla} \cdot \boldsymbol{u} \tag{1}$$

and momentum equation

$$\rho \frac{\mathrm{D}\boldsymbol{u}}{\mathrm{D}t} = -\boldsymbol{\nabla} P + \boldsymbol{\nabla} \cdot (2\mu \boldsymbol{S}) - \frac{1}{V} \sum_i \boldsymbol{F}_{p,i} \tag{2}$$

with ρ being the gas density, $\boldsymbol{u}$ the velocity, t time, μ viscosity, P pressure, V the volume of one grid cell and $\sum_i \boldsymbol{F}_p, i$ the sum of the friction forces of all particles in the grid cell. The traceless rate of strain

tensor $\boldsymbol{S}$ evaluates to

$$\boldsymbol{S} = \frac{1}{2}\left(\boldsymbol{\nabla u} + (\boldsymbol{\nabla u})^T\right) - \frac{1}{3}\boldsymbol{\nabla} \cdot \boldsymbol{u}. \tag{3}$$

In isothermal conditions the pressure is connected to the density via the speed of sound, c_s, as:

$$P = c_s^2 \rho. \tag{4}$$

Theory 2: This is typically referred to as a DNS. (resolve the bulk of all energy scales/turbulence scales?)

The evolution of the molar fraction X_∞ of a passive scalar θ is given by

$$\frac{\partial X_\infty C_g}{\partial t} + \nabla \cdot (X_\infty C_g \boldsymbol{u}) = \nabla \cdot (\rho D \nabla X_\infty) + \tilde{R}, \tag{5}$$

with D being the diffusivity, C_g the gas concentration in $^{\mathrm{mol}}/_{\mathrm{cm}^3}$ and $\tilde{R}$ a sink term, in this case only due to consumption of species θ on the surface of particles.

Theory 3: explain 5 better, C_g, X_∞??, molar fraction is not introduced

Assuming constant gas concentration and rewriting the Lagrangian derivative $\frac{\partial}{\partial t} + \boldsymbol{u} \cdot \nabla = \frac{D}{Dt}$, equation 5 simplifies to

$$\frac{DX_\infty}{Dt} = \frac{1}{C_g} \nabla \cdot (\rho D \nabla X_\infty) + R, \tag{6}$$

where $R = \frac{\tilde{R}}{C_g}$.

2.1 Particle movement

The particles are assumed to be much smaller than a grid cell and therefore treated as point particles. Each particle is tracked using a Lagrangian approach, and changes in the particle velocity $\boldsymbol{v}$ due to the force $\boldsymbol{F}_p$ acting on the particles are given by

$$\frac{\mathrm{d}\boldsymbol{v}}{\mathrm{d}t} = \frac{\boldsymbol{F}_p}{m_p}, \tag{7}$$

with m_p being the particles mass. The particle position $\boldsymbol{x}$ is then calculated accordingly:

$$\frac{\mathrm{d}\boldsymbol{x}}{\mathrm{d}t} = \boldsymbol{v}. \tag{8}$$

In this study, the only force on the particle is the drag force

$$\boldsymbol{F}_p = \frac{1}{2}\rho C_D A |\boldsymbol{u} - \boldsymbol{v}|(\boldsymbol{u} - \boldsymbol{v}), \tag{9}$$

with A being the cross section of the particle and $|\boldsymbol{u} - \boldsymbol{v}|$ the particles velocity relative to the gas flow. The drag coefficient C_D is obtained following the Schiller-Naumann correlation [9]:

$$C_D = \frac{24}{\mathrm{Re}_p}(1 + 0.15\mathrm{Re}_p^{0.687}) \tag{10}$$

which is valid for particle Reynolds numbers up to 800. The particle Reynolds number is $\mathrm{Re}_p = d_p|\boldsymbol{v} - \boldsymbol{u}|/\nu$, with $d_p = 2r_p$ being the particle diameter.

2.2 Heterogeneous reactions

We look at a simplified surface reaction system where a gas phase species θ is converted into the same amount of species γ at the particle surface, and only there. The reaction is isothermal, unimolar and only governed by the prescribed consumption rate. This can be seen as the isothermal oxygen consumption and carbon dioxide production at the surface of everlasting coal particles. The particle surface specific molar consumption rate $\dot{n}$ of species θ is

$$\dot{n} = -\lambda X_s C_g \tag{11}$$

with λ being the volumetric consumption rate of θ at the particles surface, C_g the overall gas concentration and X_s the molar fraction of species θ in the gas at the particles surface. This consumption is compensated by species θ diffusing to the particles surface from far away in the gas phase where θ has a molar fraction of X_∞. This diffusion rate is governed by

$$\dot{n} = -k(X_\infty - X_s). \tag{12}$$

The mass transfer coefficient is given by $k = \frac{C_g D Sh}{2r_p}$, where Sh is the Sherwood number. The Sherwood number is set to a constant value of 2, assuming quiescent fluid around the particle. This results in a lower mass transfer coefficient for particles that have a high relative velocity in respect to the gas. In this study, it was found that the particles Reynolds number never exceeds 5, which yields an upper limit for the underprediction of mass transfer by 50% according to the Ranz-Marshall correlation in reference [9]. Theory 5: Sh = 2???

Equations 11 and 12 can be combined to give the surface concentration for steady state as

$$X_s = \frac{kX_\infty}{C_g + \lambda k} \tag{13}$$

which can be inserted back into equation 11 to yield:

$$\dot{n} = \tilde{\lambda} X_\infty C_g \tag{14}$$

with $\tilde{\lambda} = \frac{\lambda k}{\lambda C_g + k}$ being the adapted consumption rate taking into account diffusion and consumption of θ. The source term in Eq. (5) is now given by

$$\tilde{R} = \frac{1}{V_c}\sum_{i=1}^{N_p} \dot{n}_i A_{p,i}, \tag{15}$$

where $A_p = 4\pi r_p^2$ is the particle surface area, V_c the grid cell volume and N_p the number of particles present in the grid cell. Combining Eqs. (14) and (15) yields

$$R = \frac{-1}{V_c} \sum_{i=1}^{N_p} \tilde{\lambda} X_\infty A_{p,i} \tag{16}$$

for the source term in equation 6.

2.3 Solution for homogeneous particle distribution

Averaging equation 6 over the entire volume of the domain for a homogeneous, non moving distribution of particles yields the following equation for the evolution of the mean mol fraction of θ in the flow field:

$$\frac{d\bar{X}_\infty}{dt} = -n_p \tilde{\lambda} \bar{X}_\infty \bar{A}_p \tag{17}$$

with n_p being the particle number density in the domain. Equation 17 has the analytical solution:

$$\bar{X}_\infty(t) = X_{\infty,0} \exp(-\alpha_p t). \tag{18}$$

with

$$\alpha_p = n_p \tilde{\lambda} \bar{A}_p \tag{19}$$

being the decay rate of the molar fraction X_∞ of θ.

2.4 The Stokes and Damköhler number

The Stokes number is the ratio of the particle time scale $\tau_p = \frac{S d_p^2}{18\nu}$ and the flow time scale $\tau_i = \frac{L_f}{u_{rms}}$. Particles are most efficiently captured by eddies of a similar time scale. For Stokes numbers < 1, the particles follow smaller eddies, leading to a clustering on smaller scales and therefore a more smooth distribution in the flow field, while particles with Stokes numbers > 1 would follow eddies larger than the integral scale.
Theory 6: what about large stokes numbers, define stokes number here

From τ_p and τ_i we can now construct the particle Stokes number based on the scale of the energy containing eddies.

$$\mathrm{St}_i = \frac{\tau_p}{\tau_i} = \frac{S d_p^2 u_{rms}}{18\nu L_f}, \tag{20}$$

time The particle stopping time is composed of the density ratio $S = \rho_{\text{particle}}/\rho_{\text{fluid}}$, the particles diameter d_p and the flow viscosity ν.
The chemical time scale τ_c (in which a significant change in the amount of θ is experienced) is given by the inverse of the decay rate for homogeneous particle distributions from equation 19,

$$\tau_c = \frac{1}{\alpha_p} = \frac{1}{n_p \tilde{\lambda} A_p}. \tag{21}$$

In order for the particle clustering to have a significant effect on the consumption rate, it is required that $\tau_c \leq \tau_p$. Based on the above, we define the relevant Damköhler number Da, which is the ratio of a flow time scale and the chemical time scale [10]. In our case the relevant flow time scale is the time scale of the particles τ_p, since it is the particles that cause the reaction, and the chemical time scale which is the inverse of the decay rate α. This is a significant difference from the case of homogeneous reactions, where usually the small (and fast) scales are responsible for mixing the reactants ([7], [10]). The Damköhler number is now

$$\mathrm{Da} = \frac{\tau_p}{\tau_c} = \frac{S d^2 n_p \tilde{\lambda} A_p}{18\nu} = \frac{2}{3}\frac{\overline{V}_p \tilde{\lambda} r_p S}{\nu}, \tag{22}$$

where $\overline{V}_p = \frac{4}{3}\pi r_p^3 n_p$ is the volume fraction of the particles. For the diffusion controlled regime (i.e. $\lambda C_g \gg k$), where the surface consumption rate is magnitudes higher than the diffusion rate, the Damköhler number can also written as

$$\mathrm{Da}_{\mathrm{diff.}} = \lim_{\lambda\to\infty} \mathrm{Da} = \frac{4 S r_p^2 n_p k A_p}{18\nu \overline{C_g}} = \frac{1}{3}\frac{\overline{V}_p S \mathrm{Sh}}{\mathrm{Sc}} = \frac{2\pi r_p n_p D \mathrm{Sh} \mathrm{St}_i}{u_{\mathrm{rms}} k_f}, \tag{23}$$

where Sc is the Schmidt number defined as the ratio $\frac{\nu}{D}$ of the viscosity ν and the molecular diffusion coefficient D [11].

Theory 7: define Sc+reference or remove it.

For the present study, there are two possibillities to increase the Damköhler number to higher values while holding the Stokes number constant. The most straightforward is increasing the particle number density, i.e. increasing the number of particles. Another possibility is to increase the particles radius while decreasing the particle density by the quadratic amount. In this way, the particle stopping time and the particle Stokes number is held constant , while the Damköhler number from equation 23 is changed. This approach is chosen for the highest Damköhler numbers. Since $m_{particle} \sim d^3\rho$, an increase in particle diameter results in a linear increase in mass loading, similar to the increase in the number of particles, so both ways of increasing the Damköhler number have the same effect on the mass loading. Increasing the diameter over a certain amount means violating the assumption of point particles for a small number of cells which is discussed in the results section.

8: explain why density needs to be decreased for a constant stokes number but increasing damkoehler number. Does the change in particle sizes alter the mass loading/ force coupling ratio in a different manner than altering the number of particles? What is the effect of this?

3 Study setup and studied parameters

In this study, the influence of the Damköhler number on the decay rate of a passive scalar is analysed. To do this, cases are set up where a particle-laden flow field is simulated using the open-source CFD software Pencil Code [12]. This code uses a sixth-order central difference scheme for spatial derivatives and a third-order, two stage Runge-Kutta scheme for time stepping [13].

Kinetic energy is inserted into the fully periodic domain of the simulations at large scales (close to the domain size) through a forcing function with a wavenumber of k_f. This yields turbulence without dominant directions. To compare the cases against each other, a number of non-dimensional parameters are defined, some of whom are varied while holding the others constant. The flow Reynolds number is defined as

$$\mathrm{Re} = \frac{u_{\mathrm{rms}} L_f}{\nu} \tag{24}$$

with u_{rms} being the root mean square velocity of the flow field in statistically steady state, L_f the integral scale of the flow turbulence and ν the kinematic viscosity. The same forcing is used in all cases, holding the flow Reynolds number at around 300.

Here, cases with two different Stokes numbers, 0.33 and 1.0 based on equation 20 are simulated. Table 1 shows the initial and boundary conditions used in the study. The grid spacing Δx divided by the Kolmogorov length scale $\eta = \left(\frac{\nu^3}{\epsilon}\right)^{\frac{1}{4}}$ and the particle diameter d_p can be found in table 2.

The kolmogorov scale for this flow is of the order of $2e-4$m, while the grid spacing is $\Delta x \approx 1e-3$m for the cases with the lowest resolution. An overview over the study setup can be found in tables 1 and 2. This grid spacing resolves all the the energy containing scales and all but the very smallest dissipative scales. However, since the lowest resolution is used for cases where the particle loading of the flow is low, no secondary effects of the small scale turbulence are expected, making an imperfect representation of the flow turbulence feasable. Figure 2 shows the turbulent energy spectrum of runs with different resolutions. All resolutions resolve the relevant scales of the flow.

Table 1: Boundary and initial conditions

Flow attribute	Value	Unit
$L_x = L_y = L_z$	6.28	[cm]
$N_x = N_y = N_z$	64,128,256	[-]
D	1x10^{-3}	[$^{\mathrm{cm}^2}/_{\mathrm{s}}$]
ν	2x10^{-4}	[$^{\mathrm{cm}^2}/_{\mathrm{s}}$]
N_{part}	50k-1.25M	[-]
d_{part}	30-120	[μm]
$^{\rho_{\mathrm{part}}}/_{\rho_{\mathrm{fluid}}}$	14-220	[-]
Δt	10-50	[ms]
τ_η	2.5x10^{-1}	[s]

Table 2: Grid spacing Δx vs kolmogorov scale η and default particle diameter $d_p = 50\mu m$

Resolution	$\frac{\Delta x}{\eta}$	$\frac{\Delta x}{d_p}$
64^3	5.0	32
128^3	2.5	16
256^3	1.25	8

specific p5: Add description of detailed study setup such as domain size and resolution by kolmogorov scales, as well as boundary and initial conditions, grid sensitivity

All cases are initialized and then allowed to reach a statistically steady state, at which point the concentration of the passive scalar θ is set to 1.0 throughout the domain. The mean concentration X_∞ of species θ is sampled after that. Figure 1 shows the root mean square velocity over time for cases that are only different in resolution. Data is collected 600 seconds after initialization, which is deemed sufficient to reach quasi steady state for all resolutions, as all simulations show no signs of the startup behaviour after 200 seconds. Resulting energy spectra can be seen in figure 2. The spectra are identical in the energy containing scales with slight differences in regions of high wave numbers. In the wave numbers of the scales where clustering is analysed, no differences in the spectra can be found. Together with the smooth transport of turbulent energy down the cascade without any filtering, all resolutions are deemed sufficient to resolve the relevant scales for the flow phenomena studied in this work.

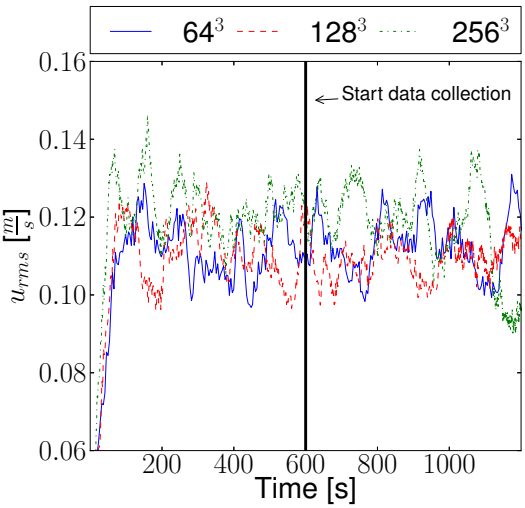

Figure 1: Root mean square of velocity in the domain for different resolutions over time.

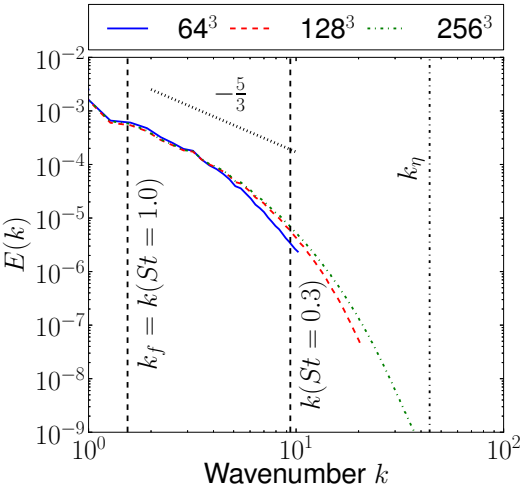

Figure 2: Turbulent energy spectra for three cases with different resolution.

3.1 Decay rate

The passive scalar decay rate can be obtained from the evolution of the averaged concentration of θ from the simulations. For all simulations, a fit using an exponential decay corresponds well with the data for all times. The volume averaged values of θ over time and its fit using a exponential function for different cases with a Stokes number of $\approx$ 1 and D =1e-3$^{\mathrm{m}^2}/_{\mathrm{s}}$ can be seen in figure 3. A higher Damköhler number results in a faster decay rate and stronger divergence from the exponential decay.

3.2 Decay rate for small Damköhler numbers

In the range of small Damköhler numbers, the particle clustering has no effect on the decay rate, since the particle number density inside the clusters is low. Accordingly, the rate can be calculated directly

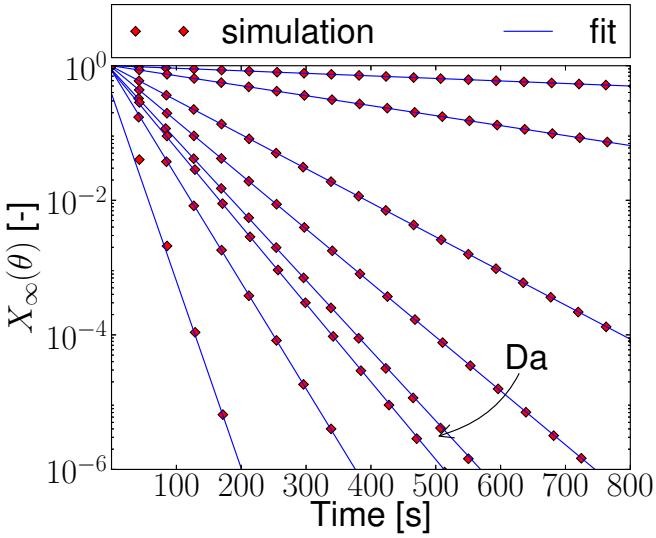

Figure 3: Influence of Damköhler number on the decay rate of the passive scalar. A higher Damköhler number results in a faster decay of passive scalar molar fraction over time.

with equation **??**. This can be inserted into equation 22 to yield

$$\alpha_p = \frac{\mathrm{Da}}{\tau_p}, \tag{25}$$

which means that for sufficiently small Damköhler numbers, the decay rate will scale linearly with Da, i.e. number of particles present in the domain.

3.3 Decay rate for large Damköhler numbers

For large Damköhler numbers, meaning a high number of particles, the particle number density inside the clusters is very high, so that internal θ is rapidly consumed. The decay rate of θ will then be limited by the diffusion of θ to the surface of the particle clusters, and the decay rate can be calculated using

$$\alpha_c = n_c \tilde{\lambda}_c \overline{A}_c, \tag{26}$$

with n_c being the number density of particle clusters in the domain. This n_c is depending on flow parameters such that

$$n_c = \left(\frac{L_x}{A_1 l} \right)^d \tag{27}$$

where the length scale of the clusters responsible for particle clustering is given by

$$l = \left(\tau_p \mathrm{u}_{rms}\right)^{3/2} \sqrt{k_f}. \tag{28}$$

Here L_x is the main length of the domain and d the dimensionality of the problem (here: 3). The size of particle clusters is an area of ongoing research [14]. How l is obtained in this study can be found in appendix A, it is the scale of the eddies with the same time scale as the particles. A_1 is a fitting parameter to account for the non-sphericity of the superparticles, for space-filling spherical superparticles it would be 1. In the cases present in this study, A_1 is $\approx 9 \ldots 11$. This corresponds to highly elongated and twisted particle clusters. Since a single particle is smaller than a grid cell, and the size of the particle clusters is of the order of the domain, the consumption rate of θ is controlled by diffusive processes, i.e.

$$\tilde{\lambda}_c = \frac{k_c}{C_g} = \frac{D_t \mathrm{Sh}}{2l}, \tag{29}$$

with D_t being the turbulent diffusivity. D_t is the sum of molecular diffusivity and convective transport of θ by eddies smaller than the eddies responsible for clustering. In our cases D_t is approximated by

$$D_t = D + \frac{u_l l}{3} \tag{30}$$

with u_l being the velocity of the eddies on the clustering length scale

$$u_l = \frac{l}{\tau_l} = u_{\mathrm{rms}}^{3/2} \sqrt{k_f \tau_p}. \tag{31}$$

For the present cases the molecular diffusivity has a larger impact than the turbulent one, as can be seen when comparing figures 7 and 8. The mean particle cluster surface area can be approximated by $\overline{A}_c = 4\pi l^2$ so that the decay rate for large Damköhler numbers becomes

$$\alpha_c = n_c 2\pi l D_t \mathrm{Sh} \tag{32}$$

which scales no longer with the number of particles and is controlled by flow field parameters.

4 Results

Results 1: Kinks in the plots should be analyzed in some way, maybe more simulations inbetween. Why not monotocially increasing with DA? Results 2: local max mass/volumeloading in some computational cells, is model still valid in these maxima?

The high Damköhler numbers can only be achieved through a high massloading of up to 1.6. Gore [15] and Kenning [16] describe how high mass loading through small particles reduces the intensity of turbulence. This effect can be seen in figures 4 and 6. Particles decrease the velocity fluctuations so that the mean u_{rms} is lower. Figure 6 shows the turbulent energy spectrum for increasing mass loading. For high mass loading, the overall turbulent energy is lower for the forcing wavenumbers and the slope of the energy cascade is slightly straitened out. Figure 5 shows the fraction of cells that contain a number of particles over the total number of cells for a simulation with 256^3 cells and 1.25 million particles with the default diameter of $50\mu m$. There are a number of cells were the assumption of non interacting point particles no longer holds, but this number is very small compared to the total number of cells and doesn't affect the flow simulation negatively, as can be seen in the turbulent energy spectrum in figure 6.

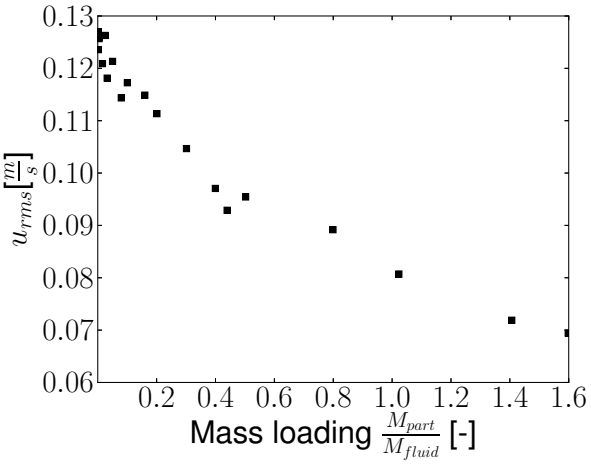

Figure 4: Massloading decreases turbulent intensity. Turbulent velocity plotted over the mass loading parameter.

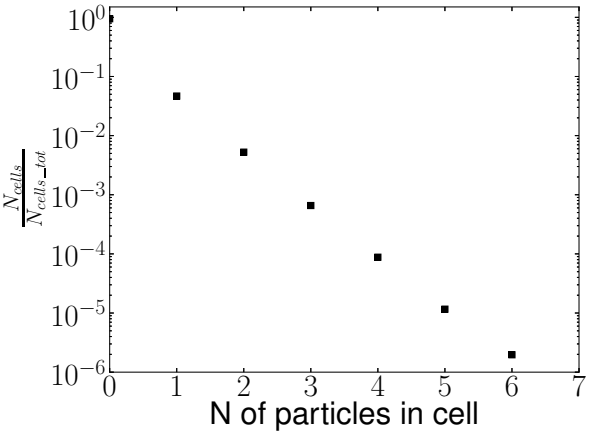

Figure 5: The fraction of cells with a high number of particles is insignificant. Fraction of cells plotted over number of particles each cell for 1.25 million particle run

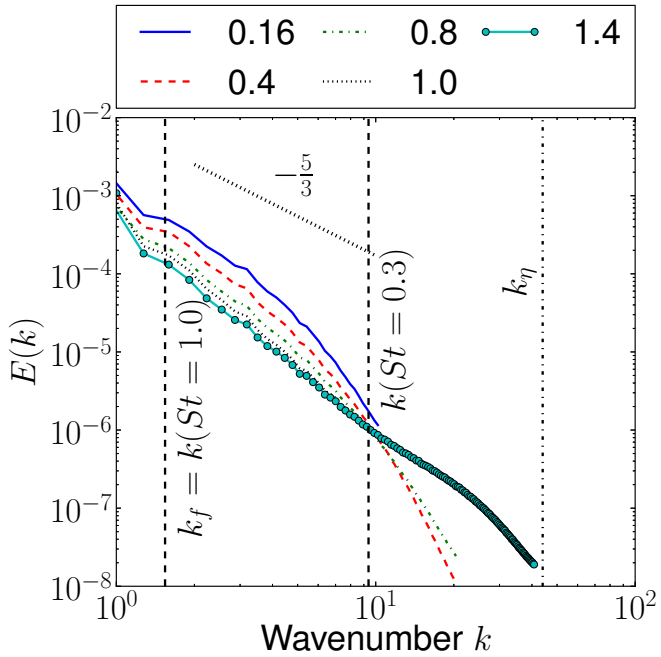

Figure 6: Turbulent energy spectra plotted for increasing mass loading $\frac{M_{particles}}{M_{fluid}}$. Increasing the mass loading decreases the turbulent energy:

The fitted decay rate over the Damköhler number for different particle Stokes numbers and molecular diffusivities can be seen in figures 7 and 8. Two distinct regimes with a transition in between can be observed: The linear scaling of the decay rate for small Damköhler numbers, and the decay rate controlled

by the particle clusters as an asymptote for high Damköhler numbers. The error bars show how the decay rate deviates from the mean fitted decay rate during each simulation. A high variance is observed when the particle number density and the resulting decay rate is high. For both diffusivities, the maximum decay rate (dotted red) is lower for the higher Stokes number. Increasing the molecular diffusivity of the passive scalar increases the overall decay rate, where a tripling of the diffusivity roughly doubles the achieved decay rate.

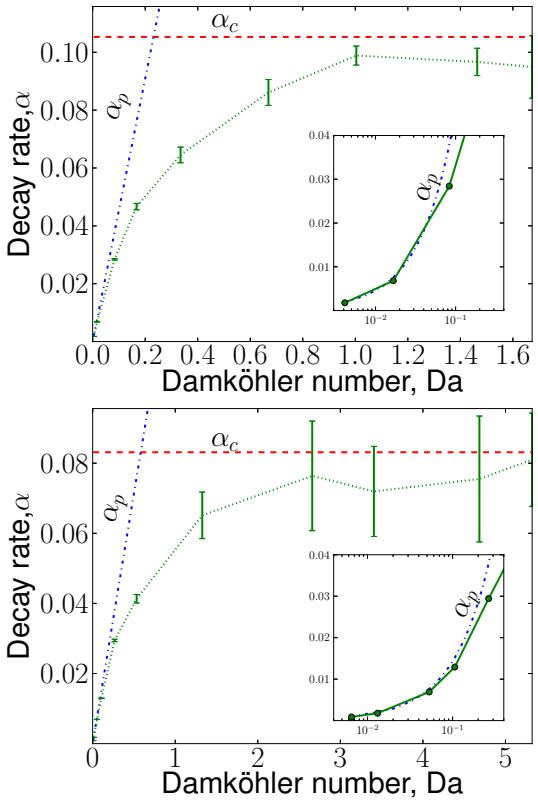

Figure 7: Influence of Damköhler number on the decay rate for St=0.3 (upper panel) and St=1.0 (lower panel). For high Damköhler numbers, the decay rate approaches a set value. $D = 10^{-3} m^2/s$

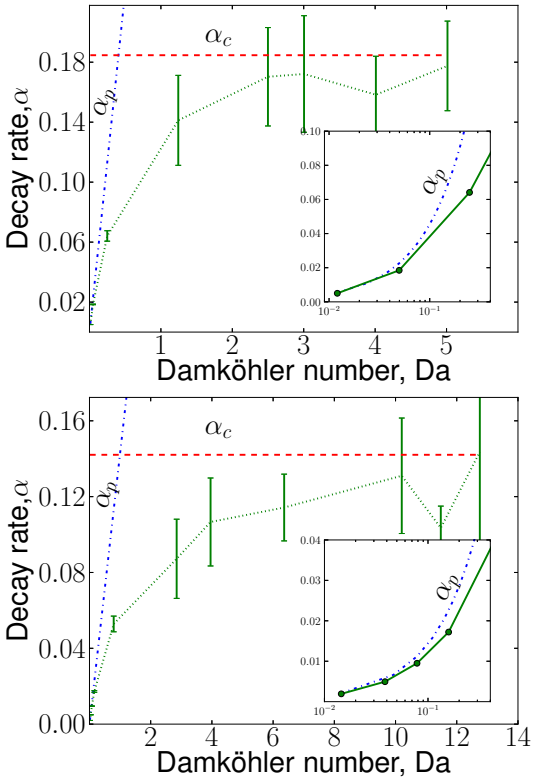

Figure 8: Influence of Damköhler number on the decay rate for St=0.3 (upper panel) and St=1.0 (lower panel). For high Damköhler numbers, the decay rate approaches a set value. $D = 3 \cdot 10^{-3} m^2/s$

5 Conclusions and future work

Particle laden flow fields with different Damköhler numbers, particle Stokes numbers and molecular diffusivities have been simulated. For all diffusivities and Stokes numbers studied, it has been found that the decay rate of the scalar scales with the Damköhler number for small Damköhler numbers, while the decay rate is independent of the Damköhler number for large Damköhler numbers. In flows with a high Damköhler number, the particle number density inside the clusters produced by the flow turbulence is so high that all gaseous reactants inside the particle clusters are rapidly consumed, but the transport of

reactants from the flow into the particle clusters is slow, severely slowing the reaction rate. The actual reaction rate (green dotted line) in figures 7 and 8 is much smaller than the reaction rate predicted by the assumption of homogeneous distribution (blue dotted line α_c). Furthermore, the deviation from the reaction rate assuming homogeneous particle distribution sets in at quite moderate Damköhler numbers. Hence, if clustering is not accounted for when modeling e.g. char surface reactions, the reaction rates can be grossly overestimated for intermediate and large Damköhler numbers.

Conclusions 2: Dependence of Particle stokes on Flow reynolds number not clear, need to define it in theory.

overall 3: extend the results section, more lines, more discussion?

Wether particles in a cell are concentrated in a cluster or evenly distributed has an impact on the resulting reaction rates. For simulations with models that do not account for local clustering in cells or in parts of the domain, the lifetime of a char particle could be severely underpredicted. This can lead to e.g. a difference in char burnout between the real application compared to its simulation in the design stage. Industrial CFD tools that employ RANS or LES models, such as Ansys Fluent [17] can be affected by this. An example is the study of Abani [3], which used Ansys Fluent with the kinetic/diffusion model introduced by Baum et al. [18].

Conclusions 1: stress clustering because of turbulence, not necessarily turbulence for species transport

The goal must now be to develop a robust model for the effect of turbulence on the heterogeneous reactions that is based on known quantities. Working towards this model, the effect of a variable Sherwood number based on the Ranz-Marshall correlation on the reaction rate has to be analysed. Furthermore, a model predicting the actual reaction rate in a simulation with turbulence and particle clusters has to be found.

Acknowledgements

The research leading to these results has received funding from the Polish-Norwegian Research Programme operated by the National Centre for Research and Development under the Norwegian Financial Mechanism 2009-2014 in the frame of Project Contract No Pol-Nor/232738/101/2014 (NELH). NELH also acknowledges the Research Council of Norway under the FRINATEK grant 231444.

A On the scale of the clustering eddies

From Kolmogorovs theory [11] we know that the eddy dissipation rate is given by

$$\epsilon = \frac{u_l^2}{\tau_l} = \frac{l^2}{\tau_l^3} = \text{constant} \tag{33}$$

with u_l being the velocity of an eddy with scale l and turnover time $\tau_l = l/u_l$. Setting up equation 33 for the eddy scale i and integral scale l and solving for the eddy scale, we get:

$$\tau_l = \tau_i \left(\frac{l}{L_i}\right)^{2/3} = \frac{l^{2/3}}{k_f^{1/3} u_{\text{rms}}}, \tag{34}$$

because from our approach in section 3 we have

$$\tau_i = \frac{1}{k_f u_{\mathrm{rms}}}. \tag{35}$$

Combining equations 34 and 35 and solving for l yields,

$$l = (u_{\mathrm{rms}}\tau_l)^{3/2}\sqrt{k_f} \tag{36}$$

when $k_f = 1/L_i$ and $\tau_l = \tau_p$.

REFERENCES

[1] International Energy Agency. World energy outlook 2013 November 2013.

[2] Silaen, A. and Wang, T. Effect of turbulence and devolatilization models on coal gasification simulation in an entrained-flow gasifier. *Int. J. Heat Mass Transf.* APR 2010 **53**:2074–2091.

[3] Abani, N. and Ghoniem, A. F. Large eddy simulations of coal gasification in an entrained flow gasifier. *Fuel* FEB 2013 **104**:664–680.

[4] Ansys Inc. Ansys 15.0 capabilities Aug 2014. Available at `http://www.ansys.com/`.

[5] Ferziger, J. H. *Computational Methods for Fluid Dynamics*. Springer Berlin Heidelberg 2002.

[6] Luo, K., Wang, H., Fan, J. and Yi, F. Direct Numerical Simulation of Pulverized Coal Combustion in a Hot Vitiated Co-flow. *Energy & Fuels* OCT 2012 **26**:6128–6136.

[7] Veynante, D. and Vervisch, L. Turbulent combustion modeling. *Prog. Energy Combust. Sci*. 2002 **28**:193 – 266.

[8] Lipatnikov, A. *Fundamentals of Premixed Turbulent Combustion*. CRC Press 2013.

[9] Tsuji, C. T. C. J. D. S. M. S. Y. *Multiphase Flows Droplets*. CRC Press 2012.

[10] Warnatz, J., Maas, U. and Dibble, R. *Combustion: Physical and Chemical Fundamentals, Modelling and Simulation, Experiments, Pollutant Formation.* Springer 2001.

[11] Pope, S. B. *Turbulent Flows*. Cambridge University Press 2000.

[12] Brandenburg, A. Pencil code homepage July 2014. Available at `http://pencil-code.nordita.org/`.

[13] Brandenburg, A. *The pencil code manual - Numerical Methods*. NORDITA July 2015. Available at `http://pencil-code.nordita.org/doc.php`.

[14] Calzavarini, E., Kerscher, M., Lohse, D. and Toschi, F. Dimensionality and morphology of particle and bubble clusters in turbulent flow. *J. Fluid Mech*. Oct. 2007 **607,**:pp.13–24,.

[15] Gore, R. and Crowe, C. Effect of particle size on modulating turbulent intensity. *Int. J. Multiph. Flow* 1989 **15**:279 – 285.

[16] Kenning, V. and Crowe, C. On the effect of particles on carrier phase turbulence in gas-particle flows. *Int. J. Multiph. Flow* 1997 **23**:403 – 408.

[17] Ansys Inc. Ansys 15.0 theory guide Aug 2014. Available at `http://www.ansys.com/`.

[18] Baum, M. M. and Street, P. J. Predicting the combustion behaviour of coal particles. *Combust. Sci. Technol.* 1971 **3**:231–243.